Theory of electronic relaxation in a metal excited by an ultrashort optical pump

V. V. Baranov and V. V. Kabanov

Department for Complex Matter, Jozef Stefan Institute, 1001 Ljubljana, Slovenia
(Received 19 August 2013; revised manuscript received 18 February 2014; published 4 March 2014)

The theory of the electron relaxation in simple metals excited by an ultrashort optical pump is developed on the basis of the solution of the linearized Boltzmann kinetic equation. The kinetic equation includes both the electron-electron and the electron-phonon collision integrals and assumes that Fermi liquid theory is applicable for the description of a simple metal. The widely used two-temperature model follows from the theory as the limiting case when the thermalization due to the electron-electron collisions is fast with respect to the electron-phonon relaxation. It is demonstrated that the energy relaxation has two consecutive processes. The first and most important step describes the emission of phonons by the photoexcited electrons. It leads to the relaxation of 90% of the energy before the electrons become thermalized among themselves. The second step describes electron-phonon thermalization and may be described by the two-temperature model. The second stage is difficult to observe experimentally because it involves the transfer of only a small amount of energy from electrons. Thus the theory explains why the divergence of the relaxation time at low temperatures has never been observed experimentally.

I. INTRODUCTION

Investigations of ultrafast nonequilibrium dynamics in metals, superconductors, and other strongly correlated systems after excitation by an ultrashort laser pulse have attracted a lot of attention during the last couple of decades. The particular interest to this field of research is related to the possibility to obtain unique information on the strength of electron-electron (e-e) and of electron-phonon (e-ph) interactions in metals and superconductors.

Up to now, detailed experimental data on relaxation processes are available for metals [1–5], high-temperature superconductors [6–13], and pnictide superconductors [14,15] using standard optical pump optical probe technique. Recently, a comprehensive analysis of experimental data on optical-pump broad-band probe in high-temperature superconductors has been performed [16]. Most of the data are analyzed in the framework of the so-called two-temperature model (TTM) [17,18] and e-ph coupling constants were obtained by using Allen's theory [19], which relates the e-ph relaxation time with the second moment, $\lambda \langle \omega^2 \rangle = 2 \int_0^\infty \alpha^2 F(\omega) \omega d\omega$, of the Eliashberg function $\alpha^2 F(\omega)$ [20,21]. The basic assumption of the model is that electrons and phonons are in a thermal quasiequilibrium (QE) at two different time-dependent temperatures $T_e(t)$ and $T_l(t)$, respectively. This assumption is correct if the e-e thermalization occurs on a much shorter time scale than the e-ph relaxation. Indeed, the QE electron distribution function, characterized by the nonequilibrium electronic temperature $T_e(t)$, nullifies the electron-electron collision integral in the Boltzmann kinetic equation (BKE) and the remaining e-ph collision integral leads to the thermalization between electrons and phonons. However, this approach has severe problems. The e-ph thermalization is $\tau_{\text{e-ph}}^{-1} \propto T^3/\omega_D^2$ in the low $k_B T < \hbar \omega_D$ limit and $\tau_{\text{e-ph}}^{-1} \propto \omega_D^2/T$ in the high $k_B T > \hbar \omega_D$ limit [19,22], where ω_D is the Debye frequency, and T is equilibrium temperature. As it was demonstrated in Refs. [4,22,23] the e-e thermalization rate $\tau_e^{-1} \propto T^2/E_F$, where E_F is the Fermi energy, is much smaller than the electron-phonon thermalization rate in the temperature range

where most of the experiments are performed $\hbar^2 \omega_D^2/E_F < k_B T < \hbar \omega_D (E_F/\hbar \omega_D)^{1/3}$. Therefore the main assumption of the TTM is not justified.

Experimentally, it was demonstrated that the electron distribution function of a laser-heated metal is a nonthermal distribution on the time scale of the e-ph relaxation time [4]. It was shown that in Ag and Au, the intensity dependence of the pump-probe signal as well as the temperature dependence of the relaxation time are inconsistent with the TTM [4]. More convincing arguments against the TTM were obtained by the direct measurements of the electron distribution function using time-resolved photoemission spectroscopy [23–25]. The interpretation of the photoemission spectra in terms of the distribution function of electrons assumes that the matrix element involved in the photoemission experiments and the density of electronic states near E_F are smooth functions of energy [26]. In the case of ordinary metals, this assumption is usually correct. In some metals, additional bands appear in the spectra, but usually these bands have relatively large excitation energy and do not influence the determination of the energy dependence of the distribution function (see Fig. 5 in Ref. [24], for example). In the measurements [23–25], the transient electron distribution function is not thermal and has high-energy tails, which survive till the thermalization occurs [23]. Moreover, in gold at about 400 fs after excitation, about 30% of the pump energy is already in the phonon subsystem [23], while the thermalization is observed only after 1 ps. Therefore the transfer of energy from electrons to phonons occurs much faster than the electronic thermalization. A similar effect is observed in Ru [24]. It is estimated that 100 fs after the pump about 20% of quasiparticles are in the high-energy tails of the distribution function. To account for this effect, it was suggested that the electron distribution function can be represented as a sum of thermal and nonthermal parts [23,24]. It was also suggested to approximate the nonthermal distribution function by a Fermi-Dirac function with reduced amplitude and a nonphysical auxiliary temperature [24]. We argue that such a decomposition is unphysical and cannot describe the electron energy relaxation. Instead the distribution

function should be determined as a solution of the complete set of BKEs.

The accurate comparison of the TTM with experimental data on Ag and Au is presented in Ref. [4]. It was experimentally demonstrated that the relaxation time decreases with temperature and does not show any pump intensity dependence contrary to the TTM predictions. In order to account for the discrepancy between the TTM and experimental data, the nonthermal electron model was introduced. This model represents the BKE for a nonequilibrium electron distribution function with electron-electron and electron-phonon collision integrals, while assuming that phonons are at equilibrium. Numerical integration of the BKEs allowed to reproduce experimental observations of the pump-probe experiments on Ag and Au. Since experimental data do not demonstrate any nonlinear effects as a function of the pump intensity the integro-differential BKE for the electrons was reduced to differential form [22]. The reduced equation is integrable and has an analytic solution. As a result it was shown again that the relaxation time should increase at low temperatures [22], contrary to the experimental results [4].

Recent analysis of the pump-probe experiments on the superconducting MgB_2 [27] and $La_{2-x}Sr_xCuO_4$ [28] has demonstrated that the superconducting order parameter is reduced due to the nonequilibrium phonons generated by the photoexcited carriers. It indicates that on the subpicosecond scale the reabsorption of the nonequilibrium phonons with the creation of low-energy electron-hole pairs is an important process that influence the energy relaxation in metals and superconductors. Note that within the nonthermal electron model, used in Refs. [4,22], this mechanism of relaxation is absent, because phonons are considered to be in equilibrium.

In this paper, we develop the theory where both nonthermal electron and phonon distribution functions are obtained by solving of linearized BKE. The e-e collisions are described on the basis of the theory, developed in Ref. [22], which explicitly accounts for the conservation of energy. In Sec. II, we derive general linearized BKE's. Then the high-temperature limit of the BKEs is derived for the Eliashberg function $\alpha^2 F(\omega) \propto \omega$, which is valid for disordered simple metals, where electrons interact with the acoustic phonons. By the direct simulations of the linearized BKEs with the different Eliashberg functions $\alpha^2 F(\omega) \propto \omega^2$ (Debye model for the acoustic phonons) and $\alpha^2 F(\omega) \propto \delta(\omega - \omega_0)$ (Einstein model for the optical phonons), we demonstrate that the derived Fokker-Planck equations describe well the energy relaxation in the high- and low-temperature range. It was also demonstrated that the energy relaxation is not sensitive to the particular form of the Eliashberg function and is determined by the second moment $\lambda\langle\omega^2\rangle$ of $\alpha^2 F(\omega)$. Note that recent results on the time-resolved angle-resolved photoemission spectroscopy (tr-ARPES) indicate that the return to equilibrium of electronic excitations is determined by the momentum and energy-dependent equilibrium self-energy [29]. Therefore the particular form of the Eliashberg function may be resolved in the tr-ARPES experiments. The accurate solution of the BKE, presented in Sec. IV, leads to a distribution function, which is very similar to that observed in the time-resolved photoemission experiments [23–25]. Then we show that the energy

transfer from the photoexcited electrons takes place on a much shorter time scale than e-e and e-ph thermalization. Therefore the main experimentally observed process is determined by the emission of phonons by the photoexcited electrons and not by the e-e or e-ph thermalization as assumed in the TTM

II. MAIN EQUATIONS

To derive linearized BKEs, describing both electron and phonon distribution functions, we start from the general BKE that takes both e-ph and e-e collision integrals into account. According to Ref. [30], the applicability of the BKE in metals is restricted by two inequalities. 1. $k_F \gg 1/l$. Here, k_F is the Fermi momentum and l is the characteristic size of inhomogeneity of the distribution function. In our case, l is restricted by the penetration depths of light or the thickness of the film. Both of them are larger than interatomic distance and therefore this condition is fulfilled. 2. $\hbar/\tau \ll E_F$. Here, τ is the characteristic timescale of the changes of the distribution function. Therefore the application of the BKE for the description of the pump-probe experiments in metals is justified on the time scale $t > \hbar/E_F = 0.1 - 1$ fs, well below the time resolution of all known experimental data discussed here. This quasiclassical description neglects any effects of quantum coherence which are not important in the case of simple metals. Therefore any effects related to the quantum coherence and dephasing are out of scope of this paper. The BKE for electrons reads

$$\dot{f}_\zeta = I_{\text{e-e}} + I_{\text{e-ph}}, \tag{1}$$

where f_ζ is the electron distribution function, averaged over the surface of constant energy,

$$f_\zeta = \frac{1}{N(\zeta)} \sum_{\mathbf{k}} \delta(\zeta_{\mathbf{k}} - \zeta) f_{\mathbf{k}}, \tag{2}$$

Note that this averaging is justified if the distribution function depends only on the electron energy $f_{\mathbf{k}} = f_{\zeta_{\mathbf{k}}}$ and does not depend on the direction of the momentum $\mathbf{k}$. For excitation by a spatially uniform fast optical pulse, it is a reasonable assumption. If the pulse did not penetrate the sample fully, the drift and the field terms should be included in the equation. In that case, the distribution function will be dependent on the direction of $\mathbf{k}$ and the expansion defined by Eq. (2) is not justified. In that case, more accurate expansions should be applied [31]. Here, $N(\zeta) \approx N(0) = m k_F/2\pi^2\hbar^2$ is the density of electronic states per spin, m is the effective mass of electron, and ζ is the electron energy counted from E_F. The density of states is a very weak function of energy and we assume that it is constant. The e-e collision integral has the form

$$I_{\text{e-e}} = \int\int\int d\zeta' d\epsilon d\epsilon' K(\zeta, \zeta', \epsilon, \epsilon') \delta(\zeta + \epsilon - \zeta' - \epsilon')$$
$$\times [f_{\zeta'} f_{\epsilon'}(1 - f_\zeta)(1 - f_\epsilon) - f_\zeta f_\epsilon(1 - f_{\zeta'})(1 - f_{\epsilon'})] \tag{3}$$

with the kernel $K(\zeta, \zeta', \epsilon, \epsilon')$ defined as

$$K(\zeta, \zeta', \epsilon, \epsilon') = \frac{2\pi}{\hbar N(\zeta)} \sum_{\mathbf{k}, \mathbf{p}, \mathbf{q}} V_c^2(\mathbf{q}) \delta(\zeta_{\mathbf{k}} - \zeta)$$
$$\times \delta(\zeta_{\mathbf{p}} - \epsilon) \delta(\zeta_{\mathbf{k}+\mathbf{q}} - \zeta') \delta(\zeta_{\mathbf{p}-\mathbf{q}} - \epsilon'). \tag{4}$$

Here, $V_c(\mathbf{q})$ is the Fourier component of the effective e-e potential. Since we consider the relaxation of nonequilibrium electron-hole excitations with energies less than E_F, we neglect all energy dependence of the kernel $K(\zeta,\zeta',\epsilon,\epsilon') \approx K \approx \pi\mu_c^2/2\hbar E_F$, where μ_c is the Coulomb pseudopotential [22]. The electron-phonon collision integral reads

$$
\begin{aligned}
I_{\text{e-ph}} = 2\pi \int d\omega \int d\zeta' Q(\omega,\zeta,\zeta') \\
\times \{\delta(\zeta - \zeta' - \hbar\omega)[(f_{\zeta'} - f_\zeta)\mathcal{N}_\omega - f_\zeta(1 - f_{\zeta'})] \\
+ \delta(\zeta - \zeta' + \hbar\omega)[(f_{\zeta'} - f_\zeta)\mathcal{N}_\omega + f_{\zeta'}(1 - f_\zeta)]\}.
\end{aligned}
\tag{5}
$$

Here, $\mathcal{N}_\omega$ is the phonon distribution function averaged over the surface of constant frequency:

$$
\mathcal{N}_\omega = \frac{1}{D(\omega)} \sum_{\mathbf{q}} \delta(\omega_{\mathbf{q}} - \omega)\mathcal{N}_{\mathbf{q}},
\tag{6}
$$

with the density of phonon states $D(\omega) = 9\omega^2/\omega_D^3$ in the Debye approximation. This averaging is also possible if the excitation pulse is spatially homogeneous and gradient terms may be omitted in the kinetic equation for phonons. The kernel of the e-ph interaction is defined as

$$
\begin{aligned}
Q(\omega,\zeta,\zeta') = \frac{1}{\hbar N(\zeta)} \sum_{\mathbf{k},\mathbf{q}} M^2(\mathbf{q})\delta(\zeta_{\mathbf{k-q}} - \zeta') \\
\times \delta(\zeta_{\mathbf{k}} - \zeta)\delta(\omega_{\mathbf{q}} - \omega).
\end{aligned}
\tag{7}
$$

Here, $M(\mathbf{q})$ is the matrix element of e-ph interaction. Because the characteristic energy of electron-hole excitations are much less than the Fermi energy, we neglect the dependence of $Q(\omega,\zeta,\zeta')$ on ζ,ζ'. As a result the e-ph collision integral is expressed in terms of the Eliashberg function [19,22]:

$$
Q(\omega,\zeta,\zeta') \approx Q(\omega,0,0) \equiv \alpha^2 F(\omega).
\tag{8}
$$

The kinetic equation for the phonon distribution function $\mathcal{N}_\omega$ reads [32]

$$
\begin{aligned}
\dot{\mathcal{N}}_\omega = 4\pi \int_{-\infty}^{\infty} d\zeta' \int_{-\infty}^{\infty} d\zeta\, Q_{\text{ph}}(\omega,\zeta,\zeta')[f_\zeta(1 - f_{\zeta'}) \\
(1 + \mathcal{N}_\omega) - f_{\zeta'}(1 - f_\zeta)\mathcal{N}_\omega]\delta(\zeta' - \zeta + \hbar\omega).
\end{aligned}
\tag{9}
$$

Note that here we neglect the anharmonic scattering of phonons which may be important at high temperatures. Here, we assume that the relaxation in the phonon subsystem is described by the inelastic phonon-electron scattering. In general, the anharmonic effects may lead to an additional temperature dependence of the relaxation time at high temperatures. The phonon-electron kernel $Q_{\text{ph}}(\omega,\zeta,\zeta') \approx Q_{\text{ph}}(\omega,0,0)$ is expressed in terms of the Eliashberg function:

$$
Q_{\text{ph}}(\omega,0,0) = Q(\omega,0,0)\frac{N(0)}{D(\omega)} = \frac{\omega_D^2 \beta}{2\hbar}\frac{\alpha^2 F(\omega)}{\omega^2},
\tag{10}
$$

here

$$
\beta = 2N(0)\hbar\omega_D/9 \sim \hbar\omega_D/E_F \ll 1.
\tag{11}
$$

Since in most of the experiments the pump-probe response is a linear function of the pump intensity [4,13], we linearize the kinetic equations. The electron and phonon distribution function have the following form:

$$
f_\zeta = f_\zeta^0 + \phi(\zeta,t),
\tag{12}
$$

$$
\mathcal{N}_\omega = \mathcal{N}_\omega^0 + \eta(\omega,t),
\tag{13}
$$

where $\phi(\zeta,t)$ and $\eta(\omega,t)$ are small nonequilibrium corrections to the equilibrium distribution functions of electrons $f_\zeta^0 = (e^{\zeta/k_BT} + 1)^{-1}$ and phonons $\mathcal{N}_\omega^0 = (e^{\hbar\omega/k_BT} - 1)^{-1}$, respectively.

In order to simplify the following calculations, we introduce the dimensionless electron energy

$$
\xi = \zeta/k_BT
\tag{14}
$$

and dimensionless phonon frequency

$$
\nu = \hbar\omega/k_BT.
\tag{15}
$$

Therefore the functions $\phi(\zeta,t) \to \phi(\xi,t)$ and $\eta(\omega,t) \to \eta(\nu,t)$.

Let us consider first the linearized e-e collision integral. The linearized BKE was derived in Ref. [22] and reduced to a differential form applying Fourier transform over energy ξ (see also Ref. [31], where a similar equation is derived for the e-e collision integral). This form of the collision integral is very useful if we consider e-e collisions only. Consideration of the e-ph interaction in the high-temperature limit leads to the differential form of the collision integral as a function of energy ξ. Therefore it is more convenient to rewrite the e-e collision integral as a function of energy ξ. Indeed, the linearized e-e collision integral has the form {Eq. (7) in Ref. [22]}

$$
\begin{aligned}
I_{\text{e-e}} = \frac{1}{\pi^2\tau_e}\Big[-\phi(\xi,t)(\pi^2 + \xi^2) \\
+ 3\int_{-\infty}^{\infty} d\xi'\phi(\xi',t)\Phi(\xi,\xi')\Big],
\end{aligned}
\tag{16}
$$

where $\tau_e = 2/K(\pi k_BT)^2$ is the e-e thermalization time, and the kernel $\Phi(\xi,\xi') = (\xi' - \xi)\{\coth[(\xi' - \xi)/2] + \tanh(\xi/2)\}$. At large $|\xi - \xi'| \gg 1$ $\Phi(\xi,\xi') \to |\xi - \xi'|$, therefore, we can simplify the e-e collision integral:

$$
\begin{aligned}
I_{\text{e-e}} = \frac{1}{\pi^2\tau_e}\Big\{-\phi(\xi,t)(\pi^2 + \xi^2) \\
+ 3\int_{-\infty}^{\infty} d\xi'\phi(\xi',t)\Phi_1(\xi - \xi') + 6\Big[E_1(\infty)\tanh\left(\frac{\xi}{2}\right) \\
- E_1(\xi) - \xi(E_0(\infty) - E_0(\xi))\Big]\Big\},
\end{aligned}
\tag{17}
$$

where the kernel $\Phi_1(x) = \frac{|x|\exp(-|x|/2)}{\sinh(|x|/2)}$ and $E_\alpha(\xi) = \int_0^\xi dx\, x^\alpha \phi(x,t)$. $E_\alpha(\xi)$ represents the dimensionless density ($\alpha = 0$) and energy ($\alpha = 1$) of nonequilibrium electrons with the energy less than ξ. This form of the e-e collision integral Eq. (17) is very easy to treat numerically since the integral part represents a convolution of the distribution function ϕ and the kernel Φ_1.

Let us turn back to the e-ph collision integrals. Substituting Eqs. (12) and (13) to Eqs. (1) and (9) yields

$$
\dot{\phi}(\xi,t) = F_1[\phi] + F_2[\eta];
\tag{18}
$$

$$
\dot{\eta}(\nu,t) = F_3[\phi] + F_4[\eta].
\tag{19}
$$

Here, the expressions for F_1 to F_4 have the following form:

$$F_1[\phi] = -\frac{\phi(\xi,t)}{\tau_1(\xi)} + \frac{2\pi k_B T}{\hbar \cosh(\xi/2)} \int_{-\infty}^{\infty} d\xi' \text{sign}(\xi - \xi')$$
$$\times \alpha^2 F\left(\frac{k_B T|\xi - \xi'|}{\hbar}\right) \frac{\cosh(\xi'/2)}{2 \sinh\frac{\xi-\xi'}{2}} \phi(\xi',t) + I_{\text{e-e}},$$

$$F_2[\eta] = \frac{2\pi k_B T}{\hbar} \int_0^{\infty} d\nu \, \alpha^2 F\left(\frac{k_B T\nu}{\hbar}\right)$$
$$\times \frac{\sinh^2(\nu/2)\tanh(\xi/2)}{\cosh(\frac{\xi+\nu}{2})\cosh(\frac{\xi-\nu}{2})} \eta(\nu,t),$$

$$F_3[\phi] = \frac{1}{2\tau_2(\nu)\nu} \int_{-\infty}^{\infty} d\xi' \phi(\xi',t) \frac{\sinh(\xi')}{\cosh(\frac{\nu+\xi'}{2})\cosh(\frac{\nu-\xi'}{2})},$$

$$F_4[\eta] = -\frac{\eta(\nu,t)}{\tau_2(\nu)}.$$

The energy dependent electron-phonon relaxation rate $\tau_1(\xi)^{-1}$ is defined as

$$\tau_1(\xi)^{-1} = \frac{2\pi k_B T}{\hbar} \int_0^{\infty} d\nu \, \alpha^2 F\left(\frac{k_B T\nu}{\hbar}\right)$$
$$\times \left[\frac{1}{\sinh\left(\frac{\nu}{2}\right)\cosh\left(\frac{\nu}{2}\right)} + \frac{\sinh^2(\xi/2)\tanh(\nu/2)}{\cosh\left(\frac{\nu+\xi}{2}\right)\cosh\left(\frac{\nu-\xi}{2}\right)}\right], \tag{20}$$

The frequency dependent relaxation rate of the phonons due to the collisions with electrons $\tau_2(\nu)^{-1}$ has the form

$$\tau_2(\nu)^{-1} = \frac{2\pi \hbar \omega_D^2 \beta}{k_B T} \frac{\alpha^2 F\left(\frac{k_B T\nu}{\hbar}\right)}{\nu}. \tag{21}$$

Note that Eq. (19) for the phonon distribution function has an analytical solution:

$$\eta(\nu,t) = \frac{1}{2\tau_2(\nu)\nu} \int_0^t dt' \exp\left[(t'-t)/\tau_2(\nu)\right]$$
$$\times \int_{-\infty}^{\infty} d\xi' \phi(\xi',t') \frac{\sinh(\xi')}{\cosh\left(\frac{\nu+\xi'}{2}\right)\cosh\left(\frac{\nu-\xi'}{2}\right)}. \tag{22}$$

Substituting it into equation (18) leads to a single integro-differential equation for the distribution function of electrons $\phi(\xi,t)$. This equation allows only numerical analysis and is therefore not very practical from the point of view of the analysis of experimental data. On the other hand, some assumption about the Eliashberg function and applying the high-temperature expansion leads to more simple equation. An important simplification is obtained if we consider the model of a disordered metal with strong phonon damping. The Eliashberg function in that limit has the following form [33]:

$$\alpha^2 F(\omega) = \begin{cases} \frac{\lambda\omega}{2\omega_D}, & \omega < \omega_D, \\ 0, & \omega > \omega_D. \end{cases} \tag{23}$$

This form of the Eliashberg function leads to a frequency independent phonon-electron relaxation rate $\tau_2^{-1} = \pi\lambda\omega_D\beta$, where the electron-phonon coupling λ is defined as

$$\lambda = 2 \int_0^{\infty} d\omega \frac{\alpha^2 F(\omega)}{\omega}. \tag{24}$$

The above equations are valid for any temperature T. Since most of the time-resolved photoemission experiments in metals are performed at temperatures above 100 K in the next section, we consider the high-temperature limit of the kinetic equation Ref. [22].

III. HIGH-TEMPERATURE LIMIT

In the high-temperature limit $k_B T > \omega_D$, the BKEs (18) and (19) can be further simplified. Let us first consider equation (19) for the phonon distribution function. In the high-temperature limit, in the expression for $F_3[\phi]$, we can neglect ν under the integral over ξ'. As the result the equation for $\eta(\nu,T)$ has the form

$$\dot{\eta}(\nu,t) = -\frac{\eta(\nu,t)}{\tau_2} + \frac{2I(t)}{\nu\tau_2}, \tag{25}$$

where the function $I(t)$ is defined by the equation

$$I(t) = \int_0^{\infty} d\xi \tanh(\xi/2)\phi(\xi,t). \tag{26}$$

This function has a very simple meaning. It describes the rate at which electrons are losing their energy to phonons {Eq. (36) in Ref. [22]}. Equation (25) defines the frequency dependence of the nonequilibrium phonon distribution function. Indeed, if we substitute

$$\eta(\nu,t) = 2p(t)/\nu \tag{27}$$

to Eq. (25), we obtain an ordinary differential equation for the function $p(t)$:

$$\dot{p}(t) = -\frac{p(t) - I(t)}{\tau_2}. \tag{28}$$

It means that at high temperatures, where $\mathcal{N}_\omega^0 \approx T/\omega$, phonons are always described by the quasiequilibrium distribution function and the function $p(t)$ describes the time evolution of the nonequilibrium phonon temperature. Substituting the phonon distribution function Eq. (27) to the equation for $F_2[\eta]$ leads to the generalized Fokker-Planck equation for the nonequilibrium electron distribution function $\phi(\xi,t)$:

$$\gamma^{-1}\dot{\phi}(\xi,t) = \frac{\partial}{\partial\xi}\left[\tanh\left(\frac{\xi}{2}\right)\phi(\xi,t) + \frac{\partial}{\partial\xi}\phi(\xi,t)\right]$$
$$+ \frac{p(t)\sinh(\xi/2)}{2\cosh^3(\xi/2)} + \gamma^{-1}I_{\text{e-e}}, \tag{29}$$

where

$$\gamma = \frac{\pi\hbar\lambda\langle\omega^2\rangle}{k_B T} \tag{30}$$

is the e-ph relaxation rate, and the e-e collision integral is given by Eq. (17). The detailed derivation of the differential form for $F_1[\phi]$ is presented in Refs. [22,34].

Note that Eqs. (28) and (29) are derived for the case of a disordered metal with electrons interacting with acoustical phonons. In the Appendix, we present the results of the numerical simulations of Eqs. (18) and (19) with three different types of Eliashberg functions at high $T > T_D$ and low $T < T_D$ temperatures, here, $T_D = \hbar\omega_D/k_B$ is the Debye temperature. We demonstrate that Eqs. (28) and (29) describe the relaxation

of the photoexcited electrons with the accuracy more than 10% in the whole temperature range provided that $\lambda\langle\omega^2\rangle$ is constant for different Eliashberg functions. It proves that Eqs. (28) and (29) are useful because they are insensitive to the approximations and assumptions that were used. It justifies their applicability for the description of the energy relaxation of optically excited electrons in a large variety of ordinary metals in the whole temperature range.

Equations (28) and (29) describe the relaxation of both phonon and electron distribution functions after perturbation. These equations represent the generalization of the TTM. The TTM may be derived from these equations in the limit when e-e relaxation is much faster than e-ph relaxation, i.e., when $\gamma\tau_e \ll 1$. It is easy to check that the equilibrium distribution functions, corresponding to the simultaneous increase of the temperature ΔT of electrons $\phi(\xi) = \frac{\Delta T}{4T}\frac{\xi}{\cosh^2(\xi/2)}$ and phonons $\eta(\nu) = \frac{\Delta T}{T\nu}$, represent a solution of Eqs. (28) and (29). Moreover, it is easy to check that the energies accumulated in the phonon and electron systems are proportional to the phonon and electron specific heats. Indeed, the energy accumulated in the phonon system is $3k_B\Delta T$. The energy in the electronic system is $2\pi^2 N(0)k_B^2 T\Delta T/3$. Therefore the energies in the phonon and electron systems are exactly proportional to their specific heats.

From Eqs. (28) and (29), we can define two dimensionless parameters. The first parameter is

$$\kappa_1 = \gamma\tau_2 = \frac{\hbar\lambda\langle\omega^2\rangle}{\lambda\omega_D k_B T\beta} \sim E_F/k_B T \gg 1. \quad (31)$$

The parameter κ_1 describes the relative time of generation of the electron-hole pairs at low energy by the hot phonons which are created by electrons at large energies. This parameter is explicitly related to the electronic C_e and phonon C_{ph} specific heats: $\kappa_1 = \frac{\pi^2 C_{ph}}{3C_e}$. The second parameter is

$$\kappa_2 = \gamma\tau_e = \frac{4\hbar^2\lambda\langle\omega^2\rangle E_F}{\mu_c^2\pi^2(k_B T)^3} \gg 1. \quad (32)$$

It describes the relative time of the electron thermalization due to e-e collision. The ratio $\frac{\kappa_2}{\kappa_1} \sim \frac{\hbar^2\lambda\omega_D^2}{\mu_c^2(k_B T)^2}$ does not contain small parameter. The order of magnitude of these dimensionless parameters for ordinary metals follows from the ratio of specific heats of electrons and phonons: $\kappa_1 \approx \kappa_2 \approx \pi^2 C_{ph}/3C_e \approx 100$. Note that parameter κ_1 is temperature-dependent.

IV. RESULTS

In this section, we discuss the results of the high-temperature limit of the theory and demonstrate TTM results obtained from the Eqs. (28) and (29) in the limit of the fast e-e relaxation. We also show that the process of emission of phonons dominates the relaxation in the low-temperature limit as well. We assume that excitation of electrons with an ultrashort laser pulse creates at $t = 0$ a broad nonequilibrium distribution of photoexcited electrons. The width of the distribution is of the order of the light frequency and is much larger than the Debye frequency ω_D. The initial distribution function after the pump pulse is approximated by the formula

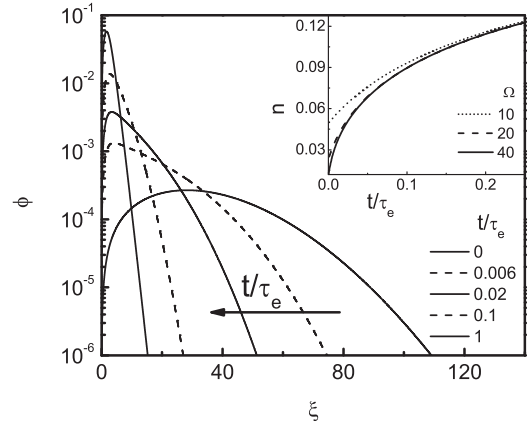$$\phi(\xi,0) = \frac{\xi}{\Omega^3}\exp(-\xi^2/\Omega^2). \quad (33)$$

FIG. 1. Evolution of the nonequilibrium distribution function by e-e collisions. The distribution function is an odd function with respect to E_F ($\xi = 0$). Inset demonstrates the time dependence of the nonequilibrium electron density for three different photon energies Ω.

Here, Ω the dimensionless excitation frequency which is defined as frequency of light measured in units of $k_B T/\hbar$. This formula preserves the energy per pulse for different frequencies of excitation Ω.

Note that this formula is different from the standard distribution of quasiparticles created by an optical pulse [35]. It has a characteristic energy which is of the order of the frequency of excitation. This function allows the existence of quasiparticles with the energy higher than Ω, but it is decreasing very quick at $\xi > \Omega$. In the Appendix, we present the results of numerical simulations assuming different initial distribution functions. The simulations show that irrespective of the particular choice of $\phi(\xi,t=0)$, the distribution function becomes independent on initial conditions on the time scale $t \sim 10^{-3}\tau_e$. Therefore the particular choice of $\phi(\xi,t=0)$ does not influence the process of energy relaxation of photoexcited electrons at the time scale longer than $10^{-3}\tau_e$.

In Fig. 1, the time evolution of the electron distribution function is presented in the absence of the e-ph interaction. The evolution is characterized by the fast reduction of the high-energy part of the distribution function and fast increase of the distribution function at small energies $\xi \sim 1$. As it follows from Fig. 1, the high-energy tails of the distribution functions disappear at the time scale determined by τ_e. This is consistent with the previous analysis of the e-e relaxation [22]. The time dependence of the density of nonequilibrium electrons, presented in Fig. 1 (inset), shows that electron thermalization occurs on the time scale of τ_e irrespective of the photon energy Ω. The difference is important only on a very short time scale for relatively low frequency Ω and is due to the fact that the initial density of nonequilibrium electrons depends on the pump frequency $n(0) \propto \Omega^{-1}$, provided that the energy per pulse is constant. Here,

$$n(t) = \int_0^\infty d\xi\,\phi(\xi,t) \quad (34)$$

is the dimensionless density of nonequilibrium electrons. The dimensionless density $n(t)$ is actually equal to the measured density of nonequilibrium electrons expressed in units of
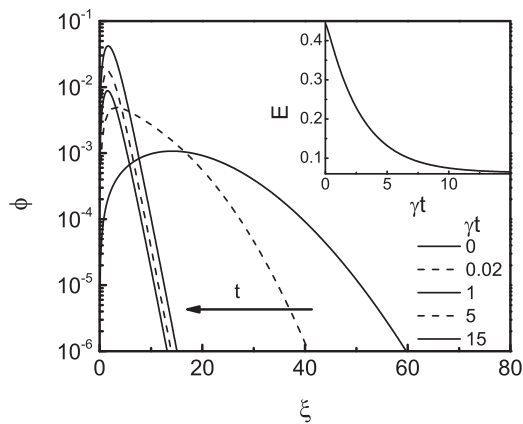
FIG. 2. Time dependence of the distribution function in the TTM limit $\kappa_1 = 20, \kappa_2 = 0.75$, and γ is the e-ph relaxation rate. Inset shows time dependence of the electron energy.
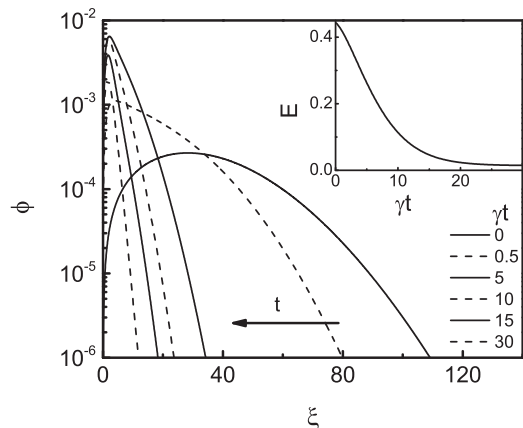

FIG. 3. Time evolution of the distribution function in the case of a metal with $\kappa_1 = \kappa_2 = 100$. Inset shows time dependence of the electron energy. By the time of the electron thermalization, 90% of energy is in the phonon subsystem. γ is the e-ph relaxation rate and $\tau_e = 100\gamma^{-1}$.

$N(0)k_BT$. Note that the scaling arguments presented in Ref. [36] predict $n(t) \propto \sqrt{t}$. Our calculations do not support this behavior. However, with the increase of $\Omega \to \infty$ the dependence of $n(t)$ becomes more and more similar to $\sqrt{t}$.

In order to demonstrate the relation of the TTM to Eqs. (28) and (29), we consider the unphysical limit $\kappa_2 = \gamma\tau_e \ll 1$. This limit corresponds to the case of the fast electron thermalization with respect to e-ph relaxation. The time evolution of the nonequilibrium distribution function $\phi(\xi,t)$ in this limit is plotted in Fig. 2. As it follows from Fig. 2, at the time scale $t \sim \tau_e = \kappa_2\gamma^{-1} \ll \gamma^{-1}$, the high-energy part of the nonequilibrium distribution function disappears and $\phi(\xi,t) = \frac{\Delta T_e(t)}{4T}\frac{\xi}{\cosh(\xi/2)^2}$. Here, $\Delta T_e(t)$ is the change of the electron temperature. This function nullifies the e-e collision integral and further evolution of the distribution function ϕ is described by the time dependence of $\Delta T_e(t)$ as it follows from Fig. 2. The ξ dependence of the distribution function at $t > \tau_e$ is always the same $\phi(\xi,t) \propto \frac{\xi}{\cosh(\xi/2)^2}$ and the evolution with time is described by the time dependent prefactor. Note that theory is linear in the excitation intensity, and therefore $\Delta T_e/T < 1$, therefore the time evolution of $\Delta T_e(t)$ is described by the linearized TTM. Note that for the case, presented in Fig. 2 $\kappa_1 = 20 \gg 1, \kappa_2 = 0.75$ the dimensionless energy density $\Delta E \approx 0.07$ transferred from electrons to phonons during the thermalization time $t \sim \tau_e$ is much smaller than the energy absorbed by electrons $\Delta E \ll E(t = 0) = 0.443$. The dimensionless energy accumulated by nonequilibrium electrons is defined as

$$E(t) = \int_0^\infty d\xi\, \xi\, \phi(\xi,t). \tag{35}$$

Therefore ΔT_e at $t \approx \tau_e$ can be evaluated using the electronic specific heat $C_e\Delta T_e = E_e$. Then thermalization between electrons and phonons occurs on the time scale $t \sim \pi^2/3\gamma$ in accordance with the TTM. The distribution function at $t \to \infty$ corresponds to $\phi(\xi,t) = \frac{\Delta T_\infty}{4T}\frac{\xi}{\cosh(\xi/2)^2}$, where ΔT_∞ is found from the equation $\Delta T_\infty(C_e + C_{ph}) = E_e$. Note that the measure for electronic temperature in that case is not the width of the distribution function but the value of $\phi(\xi,t)$ at the maximum which is approximately equal to $\Delta T/4T$. The most important property of this limit is the absence of the

high-energy tails of the distribution function, which directly follows from the fact that $\kappa_2 < 1$.

Now let us consider the more realistic case $\kappa_1 = \kappa_2 = 100 \gg 1$. These parameters roughly correspond to the case of metals like Au [23] or Ru [24]. The time evolution of the distribution function is presented in Fig. 3. At the time scale of $t \sim 15\gamma^{-1} \ll \tau_e$, the high-energy tail of the distribution function disappears and the electron distribution function can be approximated by the quasiequilibrium distribution function characterized by the electronic temperature $\phi(\xi,t) = \frac{\Delta T_e}{4T}\frac{\xi}{\cosh(\xi/2)^2}$. The electronic temperature ΔT_e is not defined by the conservation of energy, because by the time of "thermalization" about 90% of the energy has gone to phonons (see inset of Fig. 3). The dimensionless energy accumulated by nonequilibrium electrons is defined in Eq. (35). This is consistent with the time resolved photoemission data on Au [23] and Ru [24]. According to Ref. [24], the estimated electronic temperature at the peak $\Delta T_e \approx 125$ K is much less than electronic temperature estimated from TTM $\Delta T_e \approx 1200$ K. The final stage of the relaxation in that case can be characterized by the slight decrease of the electronic temperature to its equilibrium value and can be described by the TTM. Note, however, that the final stage of relaxation is very difficult to observe experimentally, because it involves the transfer of a very small amount of energy (less than 10% of the pump energy) from electrons to phonons. The biggest changes in the nonequilibrium distribution function take place during the initial stage of relaxation where the TTM is not applicable.

From these calculations, the following qualitative picture of the relaxation of the photoexcited electrons emerges. The pump pulse creates a broad distribution of electron-hole pairs with large excitation energy. The high-energy electrons relax to the low-energy scale $\zeta \sim (\hbar\omega_D E_F)^{1/2} \gg k_BT, \hbar\omega_D$ due to e-e collisions. It happens on the time scale $\langle\omega\rangle/\lambda\langle\omega^2\rangle$. The photoexited electron-hole pairs emit phonons immediately after excitation. The emission rate is temperature independent and is not affected by the Fermi distribution function, because
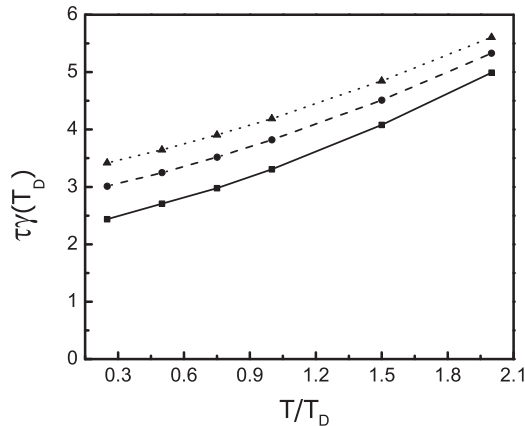
FIG. 4. Temperature dependence of the energy relaxation time for large $\kappa_1 \to \infty$ for different $\gamma(T_D)\tau_e(T_D) = 40$ (solid line), 80 (dashed line), and 120 (dotted line). $T_D = \hbar\omega_D/k_B$ is the Debye temperature.
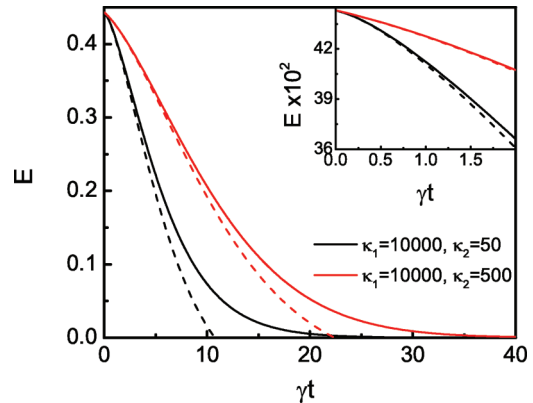

FIG. 5. (Color online) Energy relaxation in metals with large $\kappa_1 = 10000$ and different e-e relaxation times given by $\tau_e = \kappa_2\gamma^{-1}$, γ is the e-ph relaxation rate. Dashed lines represent the approximate formula (37) (see the text).

the average energy of nonequilibrium electrons is large in comparison with the phonon frequency and therefore the factor $(1 - f_{\xi-\nu})$ in the emission probability can be replaced by 1. In the Appendix, it is shown that the Fokker-Planck equation describes well energy relaxation in the low-temperature limit as well (see Figs. 8–10). The absence of the divergence of the relaxation time at low temperatures $k_B T < \hbar\omega_D$ for different e-e collision times is presented in Fig. 4. The relaxation time, defined as the time when half of the energy is transferred from electrons to phonons, is weakly temperature dependent at high-temperature and temperature independent at low temperatures. Note that electron-electron collisions have an important effect on energy relaxation. When the electron-electron collision rate increases, the high-energy excitations are decaying with the creation of more low-energy electron-hole pairs. The energy relaxation on the other hand is proportional to the number of nonequilibrium electrons. Therefore when the e-e collision rate increases the energy relaxation rate of the nonequilibrium electrons increases as well. This is demonstrated in Fig. 4. When the average energy of nonequilibrium electrons, because of emission of phonons, is reduced to the scale $\zeta \sim k_B T, \hbar\omega_D$ the $(1 - f_{\xi-\nu})$ factor becomes important leading to the strong slowing down of the relaxation, indicating the second stage of relaxation. Since most of the energy is transferred to the phonon subsystem before the time when the width of the nonequilibrium distribution function becomes of the order of $k_B T$, the final and the longest stage of thermalization is difficult to observe. In order to demonstrate that we multiply Eq.(29) by ξ and integrate over ξ from 0 to ∞ with the following result:

$$\dot{E}(t) = -\gamma[I(t) - p(t)]. \tag{36}$$

$E(t)$ is defined in Eq. (35). The e-e collision integral conserves electron energy and therefore does not contribute to Eq. (36). The first term in this equation describes the loss of the energy due to generation of phonons. The second term describes the reabsorption of phonons with the generation of low-energy electron-hole pairs and slows down the relaxation. If $\kappa_1 \gg 1$, we can neglect the second term in this equation. When the distribution function $\phi(\xi,t)$ is broad and has tails at $\xi \gg 1$, $\tanh(\xi/2)$ in the integral Eq. (26) can be replaced to 1

and therefore $I(t) \approx n(t)$, where $n(t)$ is defined in Eq. (34). Therefore Eq. (36) indicates that energy loss by electrons is proportional to the nonequilibrium electron density. In order to illustrate these arguments, we plot in Fig. 5 the time dependence of the electron energy for the case of large κ_1 in comparison with the approximate formula:

$$E(t) = E(0) - \gamma \int_0^t dt' n(t'). \tag{37}$$

As it follows from Fig. 5, this approximation describes well the time evolution of the energy until $t = (10–15)\gamma^{-1}$ when the high-energy tails in the nonequilibrium distribution function disappear. Note that the slope of the energy relaxation curve at $t = 0$ is the same in both cases (see inset of Fig. 5) because the number of photoexcited electrons is the same at $t = 0$. The difference between the two cases is due to the e-e collisions. Since for the case of $\kappa_2 = 50$ the quasiparticle multiplication is much faster the energy relaxation rate is larger. This is demonstrated in Fig. 6. The characteristic maximum in the quasiparticle density for the case of $\kappa_2 = 50$ is approximately two times larger than for the case of $\kappa_2 = 500$. Therefore the relaxation rate is determined by the
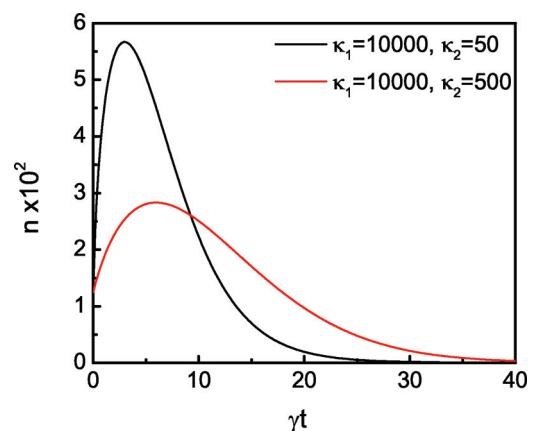

FIG. 6. (Color online) Time evolution of nonequilibrium density for the same case as Fig. 5.

nonequilibrium quasiparticle density at relatively high energy $\xi > 1$. The quasiparticle density strongly depends on τ_e. Therefore analysis of the energy relaxation after the ultrashort pump pulse allows one to obtain not only information about the e-ph interaction constant, but also about τ_e and as a consequence about the Coulomb pseudopotential μ_c.

The physical meaning of Eq. (36) is very simple. Every nonequilibrium electron emits phonons with the temperature independent rate $\tau_{\text{em}}^{-1} = \pi \lambda \langle \omega^2 \rangle / \langle \omega \rangle$. The formula for the emission rate is valid in the low-temperature limit as well. Indeed, if we consider the zero temperature limit $T = 0$ in Eq. (5) and calculate the phonon emission rate, we obtain the same expression for τ_{em} as in high-temperature limit (for details of calculations see Ref. [37]). Since the emission rate for nonequilibrium electrons is much larger than the thermalization rate in both low-temperature and high-temperature limits, we conclude that low-temperature divergence of the relaxation time will not be observed experimentally. Most of the energy will be transferred to the phonon subsystem before low-temperature relaxation processes become important. This is confirmed by the comparison of the results of calculations of the temperature dependent energy relaxation time using the Focker-Planck equation (28) and (29) with the results obtained from the kinetic equations (18) and (19) with different Eliashberg functions (Fig. 10).

Note that the theory predicts the dependence of the relaxation rate on the pump frequency Ω (Fig. 7). Indeed, preservation of the energy per pulse leads to the increase of the number of photoexcited electrons $n \propto \Omega^{-1}$. If the pump frequency is large enough, e-e collisions lead to the quick disappearance of quasiparticles with the energy higher than the threshold energy. The threshold energy is defined as the energy where the lifetime of a nonequilibrium electron due to e-e collisions becomes comparable with the lifetime due to e-ph collisions. Therefore excitation with the light frequency higher than this threshold energy does not lead to the pump frequency dependence. The situation is different when the pump frequency is below the threshold energy. In that case, the e-e collisions are not important and the relaxation rate is governed by the number of photoexcited electrons $n \propto \Omega^{-1}$, leading to the increase of the relaxation rate. This behavior is demonstrated in Fig. 7.

Experimental measurements of time-resolved photoemission in metals [23,24] provide direct information about the time-dependent nonequilibrium distribution function $\phi(\xi,t)$ (see Fig. 7 in Ref. [24]). This can be directly compared with the results of our calculations. One of the most striking resemblance between our theory and the experiments is the existence of the high-energy tails in the nonequilibrium distribution function when a substantial amount of the energy is already transferred to the phonon subsystem (Fig. 3). Very often in the experimental analysis these high-energy tails are interpreted as the nonequilibrium electron temperature ΔT_e. Usually, the results of the measurements of the nonequilibrium distribution function $f_\xi(t) = f_\xi^0 + \phi(\xi,t)$ are plotted on a logarithmic scale as a function of the energy ξ and the slope of $f_\xi(t)$ defines the nonequilibrium electron temperature $\Delta T_e(t)$ [24,25]. In this analysis, a large part of the nonthermal electrons is accounted for thermal. We suggest a different way of defining the electron temperature. In Fig. 7 of Ref. [24], the
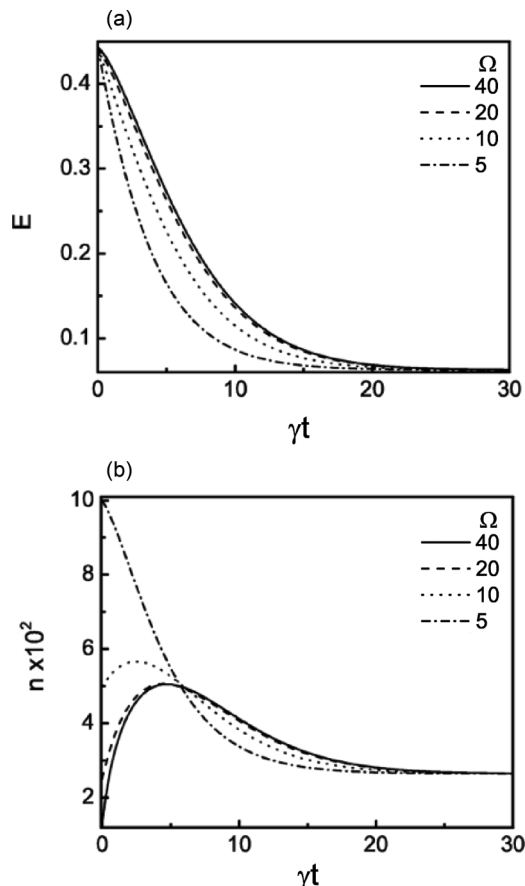

FIG. 7. (a) Energy relaxation and time dependence of (b) the nonequilibrium density for different pump frequencies Ω. When the pump frequency is relatively small the relaxation time depends on the pump frequency.

nonequilibrium part of the electron distribution function $\phi(\xi,t)$ is plotted for different time delays after pump. From this graph, it is clear that at any time delay $\phi(\xi,t) << 1$ and therefore the condition for the linearization of the BKEs is fulfilled. If $\phi(\xi,t)$ is described by the nonequilibrium temperature then $\phi(\xi,t) = \frac{\Delta T_e(t)}{4T} \frac{\xi}{\cosh(\xi/2)^2}$. The shape of ϕ in Fig. 7 of Ref. [24] is similar to that described by this formula. The function $\xi / \cosh^2(\xi/2)$ has a maximum at $\xi \approx 1.5$–1.6, which is about 1. Therefore the electronic temperature can be defined directly from the maximum of ϕ in Fig. 7 [24] $\Delta T_e(t) = 4T \phi_{\max}$, where $\phi_{\max}$ is the experimental value of the maximum of $\phi(\xi,t)$. Therefore, after 100 fs, $\Delta T_e \approx 28$ K contrary to the estimate from the slope of the distribution function $f(\xi,t)$ $\Delta T_e \approx 125$ K.

Another important consequence of the time-resolved photoemission experiments is the possibility to evaluate the electron energy and the number of the photoexcited electrons and holes. According to our theoretical results the maximum in energy and maximum in the density of photoexcited electrons should be shifted in time with respect to each other (Figs. 5 and 6). If the pump pulse is much shorter than γ^{-1}, the energy has its maximum immediately after pump pulse, because the photoexcited electrons cannot emit any phonon during the short pulse. The high-energy photoexcited electrons reduce
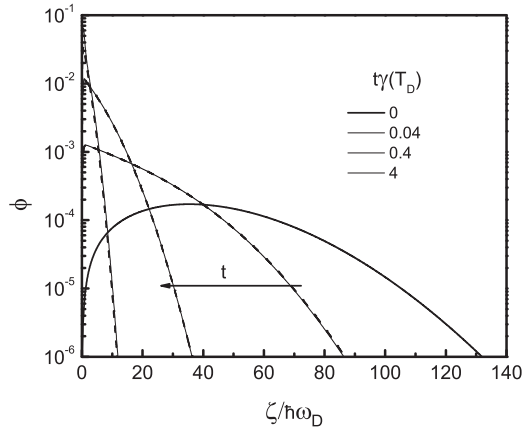
FIG. 8. Time evolution of the electron distribution function. Dashed line is from the solution of the Fokker-Plank equation (29) and solid line represents the solution of the linearized BKE Eqs. (18) and (19) with the Eliashberg function defined by Eq. (A1); $\gamma(T_D)\tau_e(T_D) = 40$.

the energy due to e-e collisions leading to an increase in the number of nonequilibrium electrons. The electron-hole recombination is slow at the short time scale because the number of nonequilibrium electrons within the energy interval $\xi < \omega_D$ is small when the pump frequency is large $\Omega \gg \omega_D$. It means that the number of photoexcited electrons increases immediately after the pump. The maximum in the nonequilibrium electron density occurs when the process of electron multiplication due to e-e collisions is compensated by the electron-hole recombination with the emission of phonons. The time when the density of the nonequilibrium electrons has its maximum indicates the end of the first stage of electron thermalization. After that, the energy relaxation rate decreases. The difference in the positions of maxima can be clearly seen in Figs. 8 and 9 of Ref. [24].
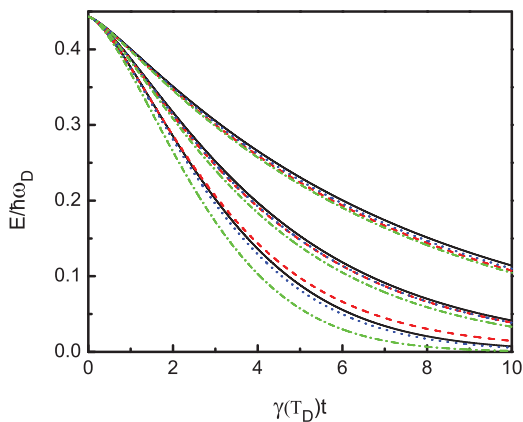

FIG. 9. (Color online) Electron energy as a function of time, calculated for different Eliashberg functions and at different temperatures $T = 2T_D$ (upper series of curves), T_D (middle series of curves), and $0.3T_D$ (lower series of curves). Solid line represents the Debye model (A1), dashed line represents the Einstein model (A2), dotted line represents the "dirty metal case" (23), and dashed-dotted line represents the energy calculated using Fokker-Planck equation (29); $\gamma(T_D)\tau_e(T_D) = 40$. In the case of the Einstein model, $T_D = \hbar\omega_0/k_B$.

Note that Eq. (36) allows the evaluation of the electron-phonon coupling constant. If we evaluate the decay rate of the electron energy experimentally and divide it with $n(t)$ on a short time scale after the maximum of the $E(t)$ curve this ratio should be constant and is exactly equal to γ. Note that the determination of the coupling constant from the single color pump-probe measurements only is problematic. The energy relaxation rate depends on the e-e and e-ph coupling constants as demonstrated in Figs. 4 and 5 and requires the knowledge of both $E(t)$ and $n(t)$ dependencies. Therefore independent measurements of the nonequilibrium density are necessary to evaluate the electron-phonon coupling constant λ.

V. CONCLUSION

We have developed the theory of the electron relaxation in metals excited by an ultrashort optical pump. The theory is based on the solution of the linearized BKE, which includes the electron-electron and the electron-phonon collision integrals. The well-known two-temperature model represents the limiting case of the theory when thermalization due to the electron-electron collisions is fast with respect to the electron-phonon relaxation.

We have demonstrated that for realistic parameters the energy transfer from electrons to phonons occurs on a timescale which is much faster than the electron thermalization. The high-energy tails in the electron distribution function disappear when most of the energy is already transferred to phonons as it is observed in the time-resolved photoemission experiments [23,24]. The reabsorption of nonequilibrium phonons slows down the relaxation.

We have demonstrated that the relaxation of the photoexcited electrons occurs in two steps. The first and the most important step represents the emission of phonons by the nonequilibrium electrons. The rate of electron energy loss at that stage is proportional to the density of nonequilibrium electrons. The temperature dependence of the relaxation at this stage is significantly different from the predictions of the two-temperature model. The density of nonequilibrium electrons is strongly influenced by the electron-electron collisions. It makes the relaxation time-dependent on the pump frequency if the pump frequency is smaller than some threshold frequency. It also allows the evaluation of the electron-phonon coupling constant λ from time-resolved photoemission data.

The second stage of the relaxation describes the electron-phonon thermalization. This stage may be described approximately by the two-temperature model. Since it involves a small energy transfer (about 10% or less) from electrons to phonons, it is difficult to observe experimentally. Our theory explains one of the most severe problems of the theory why the divergence of the relaxation time at low temperatures was never observed experimentally.

APPENDIX

In order to demonstrate that Eqs. (28) and (29) are independent of the approximations that were made, we perform extensive numerical simulations of Eqs. (18) and (19) in the limit of large $\kappa_1 \gg 1$ with three different Eliashberg functions: the linear function of phonon frequency $\alpha^2 F(\omega) \propto \omega$, Eq. (23), the Debye model

$$\alpha^2 F(\omega) = \begin{cases} \frac{\lambda \omega^2}{\omega_D^2}, & \omega < \omega_D, \\ 0, & \omega > \omega_D, \end{cases} \tag{A1}$$

and the Einstein model

$$\alpha^2 F(\omega) = \lambda \omega_0 \delta(\omega - \omega_0). \tag{A2}$$

Since the e-ph collision integral for all these cases is similar to the e-e collision integral it is very easy to treat numerically. The evolution of the nonequilibrium distribution function at low temperature $k_B T = \hbar \omega_D / 4$ is presented in Fig. 8. It is easy to see that in the whole range of time the electron distribution function calculated with Eqs. (18) and (19) with the Eliashberg function (23) is almost undistinguishable from the distribution function obtained by the solution of the Fokker-Planck equation (28) and (29). In Fig. 9, we present the electron energy as a function of time calculated on the basis of Eqs. (18) and (19) for different $\alpha^2 F(\omega)$ functions defined by Eqs. (23), (A1), and (A2) in comparison with the solution of the Fokker-Planck equation. Here, we keep $\lambda \langle \omega^2 \rangle$ constant for different Eliashberg functions. Again, the energy relaxation is almost the same for different cases in the high-temperature $k_B T > \hbar \omega_D$ region and differs not more than by 10% at low temperatures $k_B T < \hbar \omega_D$. Note that the difference between different models increases when almost all energy is transferred to phonons and electron thermalization takes place. It is because the Fokker-Planck equation overestimates the thermalization rate in the low-temperature range. On the other hand, the temperature dependence of the thermalization rate for different types of Eliashberg functions is different. In the case of the Eliashberg function defined by Eq. (23), the thermalization time is proportional to $\tau \propto T^{-2}$; in the Debye model, $\tau \propto T^{-3}$, and in the case of Einstein model related to the e-ph interaction with optical phonons, it is an exponential function of temperature $\tau \propto \exp(-\hbar \omega_0 / k_B T)$. Therefore we can conclude that energy relaxation of the photoexcited electrons is well described by the Fokker-Planck equation (29) in the whole temperature region. The relaxation does not depend on the particular form of the Eliashberg function and is defined by the second moment of the Eliashberg function $\lambda \langle \omega^2 \rangle$. The energy relaxation is not exponential, therefore we define the relaxation time as the time at which half of the absorbed energy is transferred from electrons to phonons.

The temperature dependence of the energy relaxation time is plotted in Fig. 10 for three different Eliashberg functions and for the Fokker-Plank equation. As it is clearly seen from this graph, there is marginal difference between these cases at temperatures $T > 0.2 T_D$. Therefore the relaxation time is independent of the particular form of the Eliashberg function. It is determined by the second moment of the Eliashberg function $\lambda \langle \omega^2 \rangle$ in this temperature range. It is almost independent of the particular form of the $\alpha^2 F(\omega)$ function and is not sensitive
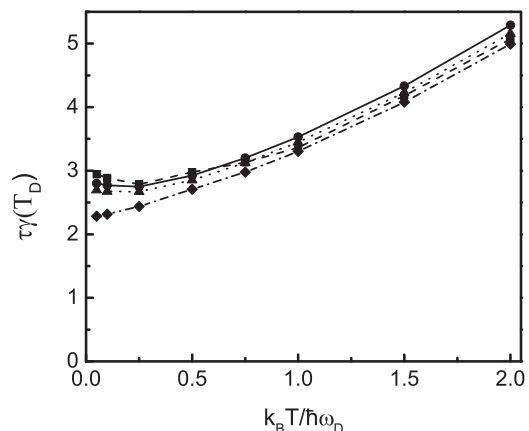

FIG. 10. Temperature dependence of the energy relaxation time calculated for large $\kappa_1 \to \infty$ for three different Eliashberg functions. Dotted line with triangles represents the "dirty metal case" (23), solid line with circles represents Debye model (A1), and dashed line with squares represents the Einstein model (A2). Solid lines with diamonds represents temperature dependence of the relaxation time for the high-temperature Fokker-Planck equation (29); $\gamma(T_D)\tau_e(T_D) = 40$. In the case of Einstein model, $T_D = \hbar \omega_0 / k_B$.

to whether the acoustic or optical phonons dominate the the relaxation, provided that $\lambda \langle \omega^2 \rangle$ is constant. Note that in the case of tr-ARPES experiments, where the relaxation time may be momentum dependent some of the features of the Eliashberg function may be resolved [29].

In the low-temperature region, there is a very small increase of the relaxation time for the Debye (2% at $T = T_D/20$) and for the Einstein(5% at $T = T_D/20$) models for the Eliashberg function. As it was mentioned in the introduction, the two-temperature model becomes valid at very low temperatures. Since the e-ph relaxation time increases exponentially with decreasing of temperature $\tau_{e\text{-ph}} \propto \exp(\hbar \omega_0 / k_B T)$ in the case of the interaction with optical phonons, the range of temperatures where the two-temperature model is efficient may be relatively broad $T < T_D/10$. In the case of interaction with the acoustic phonons, this range is more narrow. Therefore if the relaxation
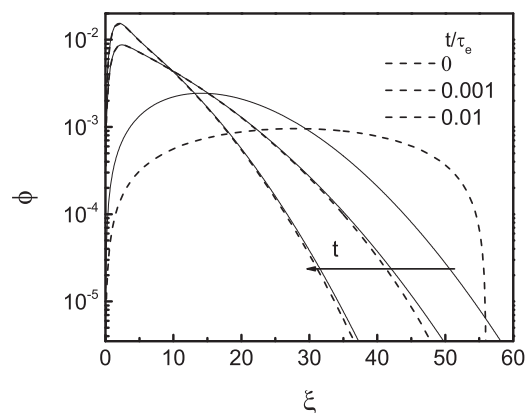

FIG. 11. Time evolution of the nonequilibrium distribution function for different initial distributions of the photoexcited electrons. Solid line corresponds to exponential distribution of the photoexcited electrons and dashed line corresponds to $\phi(\xi,0) = 12(\Omega - \xi)\xi / \Omega^4$.

is dominated by the interaction with the optical phonons it may be possible to observe the increase of the relaxation time at low temperatures. From an experimental point of view, this is very unlikely because the interaction with the acoustic phonons will dominate the relaxation at low temperatures.

In order to show that the results are independent of the initial distribution function of the photoexcited electrons, we present the results of the time evolution of the distribution function for different initial conditions $\phi(\xi,0)$. In Fig. 11, we plot the time evolution of the distribution function for

$\phi(\xi,0) = \frac{\xi}{\Omega^3} \exp(-\xi^2/\Omega^2)$ compared with the case where $\phi(\xi,0) = 12(\Omega - \xi)\xi/\Omega^4$. The results clearly demonstrate that the essential difference between these two cases survives only on the time scale less than $10^{-3}\tau_e e$ when the transfer of energy from nonequilibrium electrons to phonons is negligible. Therefore the particular choice of the initial distribution function is not important. The only important parameter is the characteristic energy scale of this distribution, which in both cases is described by the characteristic frequency Ω, which is related to the pump frequency.

[1] S. D. Brorson, A. Kazeroonian, J. S. Moodera, D. W. Face, T. K. Cheng, E. P. Ippen, M. S. Dresselhaus, and G. Dresselhaus, Phys. Rev. Lett. **64**, 2172 (1990).

[2] R. W. Schoenlein, W. Z. Lin, J. G. Fujimoto, and G. L. Eesley, Phys. Rev. Lett. **58**, 1680 (1987).

[3] H. E. Elsayed-Ali, T. B. Norris, M. A. Pessot, and G. A. Mourou, Phys. Rev. Lett. **58**, 1212 (1987).

[4] R. H. M. Groeneveld, R. Sprik, and Ad Lagendijk, Phys. Rev. B **51**, 11433 (1995).

[5] S. D. Brorson, J. G. Fujimoto, and E. P. Ippen, Phys. Rev. Lett. **59**, 1962 (1987).

[6] G. L. Eesley, J. Heremans, M. S. Meyer, G. L. Doll, and S. H. Liou, Phys. Rev. Lett. **65**, 3445 (1990).

[7] S. G. Han, Z. V. Vardeny, K. S. Wong, O. G. Symko, and G. Koren, Phys. Rev. Lett. **65**, 2708 (1990).

[8] S. V. Chekalin, V. M. Farztdinov, V. V. Golovlyov, V. S. Letokhov, Yu. E. Lozovik, Yu. A. Matveets, and A. G. Stepanov, Phys. Rev. Lett. **67**, 3860 (1991).

[9] W. Albrecht, Th. Kruse, and H. Kurz, Phys. Rev. Lett. **69**, 1451 (1992).

[10] C. J. Stevens, D. Smith, C. Chen, J. F. Ryan, B. Podobnik, D. Mihailovic, G. A. Wagner, and J. E. Evetts, Phys. Rev. Lett. **78**, 2212 (1997).

[11] J. Demsar, B. Podobnik, V. V. Kabanov, T. Wolf, and D. Mihailovic, Phys. Rev. Lett. **82**, 4918 (1999).

[12] V. V. Kabanov, J. Demsar, B. Podobnik, and D. Mihailovic, Phys. Rev. B **59**, 1497 (1999).

[13] C. Gadermaier, A. S. Alexandrov, V. V. Kabanov, P. Kusar, T. Mertelj, X. Yao, C. Manzoni, D. Brida, G. Cerullo, and D. Mihailovic, Phys. Rev. Lett. **105**, 257001 (2010).

[14] L. Stojchevska, P. Kusar, T. Mertelj, V. V. Kabanov, X. Lin, G. H. Cao, Z. A. Xu, and D. Mihailovic, Phys. Rev. B **82**, 012505 (2010).

[15] L. Rettig, R. Cortes, S. Thirupathaiah, P. Gegenwart, H. S. Jeevan, M. Wolf, J. Fink, and U. Bovensiepen, Phys. Rev. Lett. **108**, 097002 (2012).

[16] S. Dal Conte, C. Giannetti, G. Coslovich, F. Cilento, D. Bossini, T. Abebaw, F. Banfi, G. Ferrini, H. Eisaki, M. Greven, A. Damascelli, D. van der Marel, and F. Parmigiani, Science **335**, 1600 (2012).

[17] M. I. Kaganov, I. M. Lifshits, and L. B. Tanatarov, Zh. Eksp. Teor. Fiz. **31**, 232 (1956) [Sov. Phys. JETP **4**, 173 (1957)].

[18] S. I. Anisimov, B. L. Kapeliovich, and T. L. Perel'man, Zh. Eksp. Teor. Fiz. **66**, 776 (1974) [Sov. Phys. JETP **39**, 375 (1974)].

[19] P. B. Allen, Phys. Rev. Lett. **59**, 1460 (1987).

[20] G. M. Eliashberg, Sov. Phys. JETP **11**, 696 (1960) [Zh. Eksp. Teor. Fiz. **38**, 966 (1960)].

[21] G. M. Eliashberg, Sov. Phys. JETP **12**, 1000 (1961) [Zh. Eksp. Teor. Fiz. **39**, 1437 (1960)].

[22] V. V. Kabanov and A. S. Alexandrov, Phys. Rev. B **78**, 174514 (2008).

[23] W. S. Fann, R. Storz, H. W. K. Tom, and J. Bokor, Phys. Rev. B **46**, 13592 (1992).

[24] M. Lisowski, P. A. Loukakos, U. Bovensiepen, J. Stahler, C. Gahl, and M. Wolf, Appl. Phys. A **78**, 165 (2004).

[25] L. Perfetti, P. A. Loukakos, M. Lisowski, U. Bovensiepen, H. Eisaki, and M. Wolf, Phys. Rev. Lett. **99**, 197001 (2007).

[26] F. Reinert, S. Hüefner, in *Very High Resolution Photoelectron Spectroscopy*, edited by S. Hüefner (Springer, Berlin Heidelberg), 2007.

[27] J. Demsar, R. D. Averitt, A. J. Taylor, V. V. Kabanov, W. N. Kang, H. J. Kim, E. M. Choi, and S. I. Lee, Phys. Rev. Lett. **91**, 267002 (2003).

[28] P. Kusar, V. V. Kabanov, S. Sugai, J. Demsar, T. Mertelj, and D. Mihailovic, Phys. Rev. Lett. **101**, 227001 (2008).

[29] M. Sentef, A. F. Kemper, B. Moritz, J. K. Freericks, Z.-X. Shen, and T. P. Devereaux, Phys. Rev. X **3**, 041033 (2013); J. A. Sobota, S.-L. Yang, D. Leuenberger, A. F. Kemper, J. G. Analytis, I. R. Fisher, P. S. Kirchmann, T. P. Devereaux, and Z.-X. Shen, J. Electron Spectrosc. Relat. Phenom. (2014), doi:10.1016/j.elspec.2014.01.005.

[30] E. M. Lifshitz, L. P. Pitaevskii, *Statistical Physics, Part 2* (Pergamon Press, Oxford (1980).

[31] H. Smith and H. H. Jensen, *Transport Phenomena* (Clarendon Press, Oxford, 1989).

[32] E. M. Lifshitz and L. P. Pitaevskii, *Physical Kinetcs* (Pergamon Press, Oxford, 1981).

[33] D. Belitz, Phys. Rev. B **36**, 2513 (1987); D. Belitz and M. N. Wybourne, *ibid.* **51**, 689 (1995); B. I. Belevtsev, Yu. F. Komnik, and E. Yu. Beliayev, *ibid.* **58**, 8079 (1998).

[34] V. E. Gusev and O. B. Wright, Phys. Rev. B **57**, 2878 (1998).

[35] V. F. Elesin and Yu. V. Kopaev, Sov. Phys. Uspekhi **24**, 116 (1981).

[36] G. Tas, H. J. Maris, Phys. Rev. B **49**, 15046 (1994).

[37] M. Beyer, D. Stadter, M. Beck, H. Schafer, V. V. Kabanov, G. Logvenov, I. Bozovic, G. Koren, and J. Demsar, Phys. Rev. B **83**, 214515 (2011).